Analysis of immersed silica optical microfiber knot resonator and its application as a moisture sensor

Marcelo A. Gouveia,[1] Paloma E. S. Pellegrini,[1] Juliana S. dos Santos,[2] Ivo M. Raimundo, Jr.,[2] and Cristiano M. B. Cordeiro[1,*]

[1]Institute of Physics "Gleb Wataghin", University of Campinas, Unicamp, Campinas, Brazil

[2]Institute of Chemistry, University of Campinas, Unicamp, Campinas, Brazil

*Corresponding author: cmbc@ifi.unicamp.br

Received 8 August 2014; revised 29 September 2014; accepted 5 October 2014; posted 6 October 2014 (Doc. ID 220507); published 29 October 2014

An embedded silica optical microfiber knot resonator humidity sensor is presented. As silica has a poor response to environmental humidity changes, a surrounding layer of Nafion is used as a transducer. Spectral characterization and also a procedure to determine the coupling and total loss coefficients are presented. Sensitivity as high as (0.29 ± 0.01) nm/% relative humidity has been noticed. Possible issues that emerge from the use of Nafion such as bulk swelling, refractive index hysteresis, as well as a saturation process, are discussed. © 2014 Optical Society of America

OCIS codes: (060.2370) Fiber optics sensors; (160.5470) Polymers; (230.5750) Resonators; (310.6845) Thin film devices and applications.

http://dx.doi.org/10.1364/AO.53.007454

1. Introduction

Silica optical fibers have proved to be an excellent platform for sensing mainly because of their lifelong durability, toughness, and distributed and passive measurements. Interferometer fiber-based devices are powerful tools for sensing as the sensitivity is based on phase shifts of the light traveling through the device. As examples, fiber Bragg grating Fabry–Perot cavities [1] and long period grating Mach–Zehnder interferometers [2] could be cited. Another kind of interferometer widely used for sensing purposes is the multimodal one, in which interference occurs between traveling modes [3]. The development of techniques to produce low-loss microfibers from standard fibers allowed these sensors to have their sensitivity enhanced as a consequence of the stunning properties inherent to those micrometric fibers [4,5], such as high associated evanescent field and dispersion engineering. Directly connected to this class of microwaveguides, microfiber optical resonators could be introduced. Generally, they are sorted into three subclasses: micro loop resonators [6], micro coil resonators [7], and micro knot resonators (MKRs) [8]. Although their spectral response as well as their theoretical model are approximately similar and they have been widely investigated for sensing purposes, each of them can be applied to specific areas of interest, such as nonlinear effects [9], fluidic and current sensing [10,11], and laser cavity [12].

For some sorts of applications, a transducer must be applied to convert insensitive changes into ones that are measurable in standard silica fiber-based devices. One of these applications is related to moisture measurement, which is compulsory to have a sensitive medium to act as a transducer to any environmental humidity change, giving a measurable response, which would then be transformed into an optical signal. Solutions for this present argument have been reported using coatings [13–18] and special polymeric microfibers [19,20].

One possible transducer, Nafion, seems to be an interesting choice due to its high hydrophilicity,

1559-128X/14/317454-08$15.00/0

chemical and thermal stability, high conductivity, mechanical toughness, high adherence to silica, and low refractive index. This perfluorosulfonated-based polymer is assembled by DuPont and has been explored for the development of optical [18] and electrochemical [21] sensors as well as in fuel cell technology [22,23], as it is a proton exchanger due to its sulfonate groups. Conceptually, its molecular structure is formed by a hydrophobic backbone with chains containing sulfonate end groups that bring hydrophilicity to the polymer.

This paper introduces the MKR feature of relative humidity (RH) sensor using Nafion as a coating, which would be under the influence of moisture changes. Intrinsic to these changes, the polymer layer would have its refractive index and the tensile or compressive stress either reduced or increased. Such effects result from the hydrophilic character of Nafion, where the material can either swell or shrink with absorbed water change. The refractive index is also able to change, since the material composition changes locally.

Initially, the MKR and its fabrication method will be described [24], followed by how its coupling and total loss coefficients behave at certain immersed conditions [25–28]. Then, an embedded silica optical MKR humidity sensor will be presented. Also, a discussion on how the polymer humidity dependence affects the modal propagation and the structure of the MKR is carried out. The film refractive index tendency in the presence of humidity changes is characterized by the Abelès method [29]. Drawbacks such as anomalous bulk refractive index deviation as well as swelling that could raise hysteresis behavior and the saturation process are investigated.

2. Micro Knot Resonator: Manufacturing and Spectral Tuning

A. Manufacturing

As a requirement for manufacturing MKRs, low-loss microfibers are, generally, produced by the brush flame technique, in which a standard optical fiber is pulled down and heated up at a certain temperature in a certain region, producing the so-called fiber taper. The fiber taper shape was described in detail by Birks and Li [30]. Characteristics such as high modal density as well as strong evanescent field are located on the waist region, also called the microfiber, and nearby, on the transition, where it becomes gradually thinner. Figure 1(a) presents a schematic of a typical taper.

Generally, MKRs are produced from microfibers with diameter smaller than 5 μm due to their considerable associated evanescent field that allows the device to constitute a resonant field. In addition, fiber taper for such purpose usually has a waist zone, at least 4 mm long, which is a sufficient condition to produce a MKR totally located at the waist region for a wide range of the resonator's diameter, from, approximately, 150 μm to 1 mm, without considerable

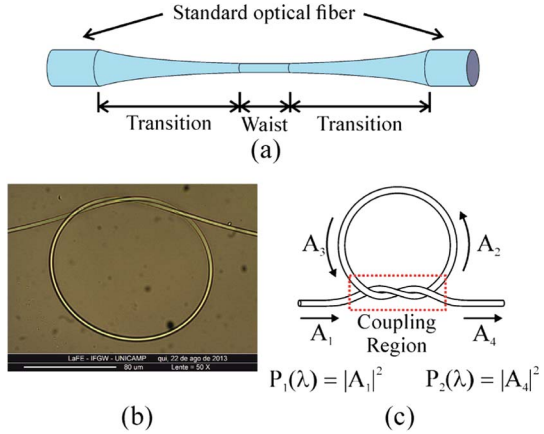

Fig. 1. (a) Example of a typical fiber taper. (b) A 50× optical microscopy of a MKR made from a 3 μm thick microfiber. (c) MKR schematic that shows modal amplitudes associated with the resonant and straight regions of the device as well as the coupling region that connects these two regions.

associated curvature losses. Moreover, this length allows microfibers to present good mechanical bending resistance, indispensable during the manufacturing process. Although the literature suggests, for better modal coupling, that the coupling region should be composed by the transitions instead of just the microfiber [31], this study just focuses on the MKR entirely inside the waist region for simplicity.

The microfiber is first produced inside a huge fiber knot, where both ends are placed and held on two stages, which travel oppositely. In this way, the knot is pulled down carefully to the desired diameter and placed naturally at the center of the waist region [24]. As this method produces double-ended MKR, all spectral changes can be monitored during the manufacturing, which results in a preliminary control over spectral attributes that are being sorted. Finally, the MKR is placed on a low refractive index substrate, which could be either an MgF_2 plate or a polymeric low refractive index ($n = 1.33$) thin film produced by spin cast on a microscope slide. Figure 1(b) presents a typical double-ended MKR made from a 3 μm thick microfiber supported on a low refractive index polymer-based substrate. Possible issues caused by these supporting substrates, such as induced birefringence as well as scattering losses, are considered in following analysis.

B. Spectral Tuning

The associated fields of a typical MKR have their amplitudes presented in Fig. 1(c). Note that MKR has two particular regions: cavity and coupling regions. On the cavity, there are two distinguished resonant complex amplitudes, A_3 and A_2, where their ratio is given by $\mathrm{Exp}(i\tilde{\beta}(\lambda)L_{\mathrm{cav}})$, with $\tilde{\beta}(\lambda) = \beta(\lambda) + i\alpha(\lambda)$. The real part, $\beta(\lambda)$, is the mode propagation constant and defines the phase addition per unit of length traveled by a certain allowed mode. The imaginary part, $\alpha(\lambda)$, defines the total attenuation loss per length. The cavity length is expressed as L_{cav}. Therefore, the

total loss coefficient could be expressed as $\boldsymbol{a} = \mathrm{Exp}(-\alpha(\lambda)L_{\mathrm{cav}})$.

Related to the coupling region, the coupling coefficient, $\boldsymbol{t}$, is defined as the ratio of power traveling in both twisted waveguides in the coupling region, where, initially, all power was localized just in one waveguide. This coefficient behaves roughly periodically as function of wavelength or, more explicitly, $\boldsymbol{t} \propto \mathrm{Sin}(C_0(\lambda)L_{\mathrm{coupler}})$, where C_0 is the power exchanging coefficient and L_{coupler}, is the coupling region length.

With the associated amplitudes shown in Fig. 1(c) and the conditions presented on this topic, using a transfer matrix method, the spectral output of a typical single-mode MKR is given by [28]

$$P(\lambda) = \frac{t^2 + a^2 - 2ta\,\mathrm{Cos}(\beta(\lambda)L_{\mathrm{cav}})}{1 + t^2a^2 - 2ta\,\mathrm{Cos}(\beta(\lambda)L_{\mathrm{cav}})}, \tag{1}$$

where $P(\lambda) = P_2(\lambda)/P_1(\lambda)$. From this expression, all spectral attributes could have their theoretical expressions solved as function of $\boldsymbol{t}$, $\boldsymbol{a}$, $\beta(\lambda)$, and L_{cav}. More explicitly, the mode propagation constant could be written as $\beta(\lambda) = 2\pi n_{\mathrm{eff}}/\lambda$, where n_{eff} is the effective refractive index of the mode. The free spectral range (FSR) is obtained directly by equaling the phase difference to 2π, which yields the FSR expression $\mathrm{FSR} = \lambda^2/n_{\mathrm{eff}}L_{\mathrm{cav}}$. Other spectral parameters such as *finesse* [the ratio of the FSR and the full width at half-maximum (FWHM)] $f = \mathrm{FSR}/\mathrm{FWHM}$, and the extinction ratio (ratio of the off-resonance and the on-resonance power), $\varepsilon = P_{\mathrm{max}}/P_{\mathrm{min}}$, are obtained directly from expression (1) and given, respectively, by the following expressions:

$$f = \frac{\pi\sqrt{ta}}{1 - ta}, \tag{2}$$

$$\varepsilon = \left[\frac{(t + a)(1 - ta)}{(t - a)(1 + ta)}\right]^2. \tag{3}$$

Note that, as in expression (1), $\boldsymbol{t}$ and $\boldsymbol{a}$ remain commuting in expressions (2) and (3). In fact, the determination of those coefficients cannot be performed unless a well-known condition is considered. Mckinnon *et al.* have presented a straightforward method to determine them, solving both expressions (2) and (3) consistently, by observing the spectral dependency of the coupling coefficient, $\boldsymbol{t}$, and considering that the losses, $\boldsymbol{a}$, shall be a weak function of wavelength and, therefore, treated as a constant [25]. Equation (4) introduces the solution for both $\boldsymbol{t}$ and $\boldsymbol{a}$, from expressions (2) and (3) and this ambiguous character,

$$(t, a)^{\pm} = \left\{\left(\frac{\varepsilon + \rho}{\varepsilon - \rho}\right) \pm \left[\left(\frac{\varepsilon + \rho}{\varepsilon - \rho}\right)^2 - 1\right]^{\frac{1}{2}}\right\}^{\frac{1}{2}} \sqrt{\tau}, \tag{4}$$

where

$$\rho = \left(\frac{1 - \tau}{1 + \tau}\right)^2,$$

$$\tau = t \cdot a = \left\{\left[\left(\frac{\pi}{2f}\right)^2 + 1\right]^{\frac{1}{2}} - \frac{\pi}{2f}\right\}^2.$$

Note that Eq. (4) just splits the product $\boldsymbol{ta}$.

With a slight modification of the method described by Mckinnon *et al.* for determining $\boldsymbol{t}$ and $\boldsymbol{a}$ [23], regarding the good mechanical stability inherent to this class of resonator, two MKR samples have been immersed into two liquids, water and ethanol, to have their coupling and total losses coefficients evaluated. At 1550 nm, water and ethanol possess refractive indices of $n_{\mathrm{water}} = (1.3167 \pm 0.0004)$ and $n_{\mathrm{ethanol}} = (1.3522 \pm 0.0003)$, and the water absorbance is, approximately, 6 dB greater than that of ethanol [32].

On the one hand, simulations using the commercial software of finite element COMSOL have been performed and have shown that for a 65 μm straight coupler with 3 μm thick microfibers—values of coupler length and microfiber diameter were chosen according to the resonator's dimensions—with no separation from each other, completely immersed in ethanol and water, the coupling parameter has varied just 0.04 in its absolute value. In addition, the twist character of the coupling region can raise the effect of coupling between fields with different polarization states. Such effect, however, can be neglected since it would only be considerable for a several millimeter long twisted coupler made from 3 μm diameter microfibers [33,34]. Moreover, for a twisted coupler with the same attributes as above, the beating lengths for each polarization state (x and y), also simulated using COMSOL, are about 85 and 87 μm for ethanol and 88 and 92 μm for water. As the beating lengths are close to one another, and the real coupler length is smaller, the coupling coefficients are likely degenerated, being able to be evaluated as just one, neglecting local effects of polarization, resulting in a polarization insensitive MKR.

On the other hand, it is indeed expected that the total losses change as the external medium is changed from water to ethanol, as their intrinsic absorbance differs considerably. In addition, the curvature losses should be greater as long as the ratio between the internal and outer refractive indices tends to the unity. As the deviation between both indices is about 2.5%, the curvature losses can be overcome by the absorption one. Therefore, it is predicted that the total loss coefficient varies as the surrounding medium is changed, while the coupling coefficient remains fixed. Clearly, all these conditions are satisfied if, and only if, the MKR is kept motionless. In order to perform the experiment, a simple setup was considered: the MKR is supported on a low refractive index polymeric thin film ($n = 1.33$) and an interrogation unit that launches a broadband light signal, from 1500 to 1600 nm, into the device and analyzes the output spectrum with maximum resolution of 10 pm.

Figure 2(a) presents three spectra from the same sample immersed in three different media. Each resonance of the two immersed cases had its characteristics (finesse and extinction ratio) evaluated, as shown in Fig. 2(b). Making use of Eq. (4), the pair $\{(t,a)^+;(t,a)^-\}$ could be evaluated and, according to the hypothesis of losses discussed above, was uniquely determined. The spectral dependence of t and a is shown in Fig. 2(c). This method was applied to evaluate such coefficients for the two MKR samples, S1 and S2, as pointed out previously. All averaged collected parameters as well as the averaged coupling and attenuation coefficients are listed in Table 1.

Observing the state diagram (Fig. 3) of the MKRs (built using both finesse and extinction ratio) the state in which the resonator is found is one of the intersections of these associated curves. As can be seen, the path made by each resonator state (S_1 or S_2) is almost vertical, indicating that the coupling coefficient is approximately constant while the attenuation coefficient experiences an expressive change.

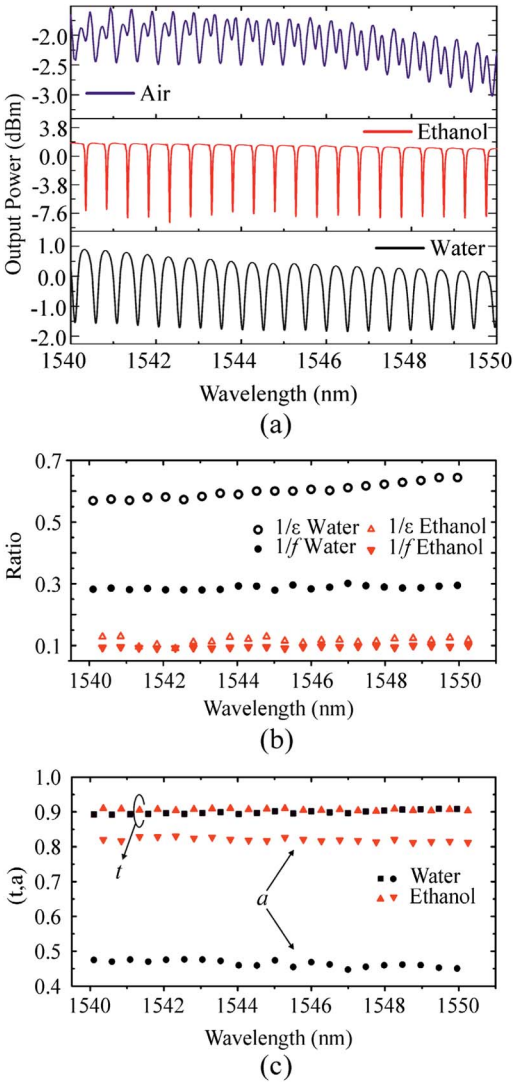

Fig. 2. (a) Spectral shapes of the sample 1 for three distinguished conditions: surrounded by air, ethanol and water. (b) Inverse of the extinction ratio and finesse of each resonance obtained directly from the spectra. (c) Coupling and attenuation losses evaluated using equation (4) from the extinction ratio and finesse.

Table 1. Spectral Characteristics and Evaluated Coupling and Attenuation Coefficients from Two Immersed MKRs

Sample	S1		S2	
Medium	Water	Ethanol	Water	Ethanol
FSR (nm)	0.49	0.49	0.81	0.81
FWHM (nm)	0.14	0.05	0.13	0.09
$Q(\times 10^4)$	1.09	3.29	1.20	1.73
f	3.49	10.51	6.27	8.89
ε	1.67	8.47	2.09	2.33
t	0.90	0.90	0.93	0.94
a	0.46	0.82	0.66	0.75

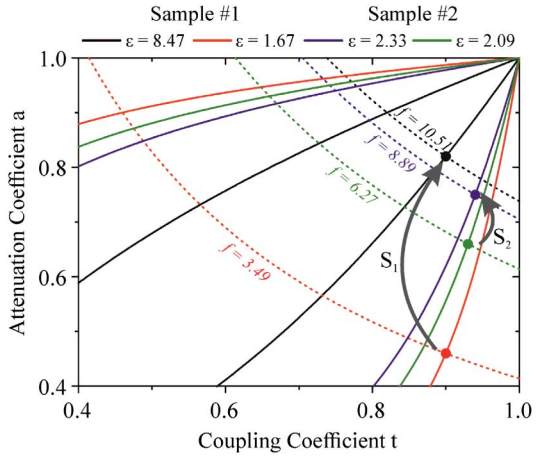

Fig. 3. State (t-a) diagram of the two analyzed samples. Solid and dashed lines represent the extinction ratio and finesse geometric locals, respectively. Gray arrows depict the path made by each sample when the environment changes from water to ethanol.

Due to the substrate-induced birefringence as well as high-order modes allowed, the air surrounding the MKR spectrum is considerably noisy. As long as the surrounding medium is changed or, more explicitly, the refractive index approximates the substrate one, less noise is observed, extinguishing the observable induced birefringence. Whether the chosen material has smaller absorbance coefficient, both finesse and resonance depth would increase, as observed in Fig. 2(a) and listed in Table 1.

This method suggests spectral tuning and modal filtering by immersing MKR. From this approach, such devices turn out interestingly, bringing a wealth of applications such as cavity tuning, tunable wavelength filtering, and sensing.

3. Humidity Sensor based on MKR Coated with Nafion

A. Nafion as an Active Medium for a MKR Sensor

Nafion is a perfluorosulfonated-based polymer constituted by two main parts: hydrophilic perfluorosulfonic chains with sulfonate end groups and a hydrophobic perfluorinated backbone. With this antagonistic structure, this polymer has some

interesting properties such as structural dependence on humidity shifts. Although the structural behavior of such a polymer remains unclear, it is sufficient to say for this study that the polymer, during the process of water absorption, increases its spatial dimensions and the bulk refractive index decreases, since the Nafion dried bulk index is about 1.38 and the water one is about 1.33 at 633 nm [35].

As a result of the manufacturing process, the refractive index varies with the thickness, since the refractive index depends on how the polymer is organized into thin films. Nafion thin films greater than 1000 nm have their refractive indices compared to the bulk one. Besides, hysteresis and birefringence could be found as the material does not have the same structural organization on each axis and it could change after several tryouts.

To measure the refractive index of thin homogeneous Nafion films, an optical technique based on the Abelès method was used [29]. The experimental setup is formed by a linearly polarized He–Ne laser with TM polarization state (electric component perpendicular to the incident plane), which is aimed at the sample, and then its reflection is collected by a detector to be analyzed. Initially, the substrate is placed on a rotational stage and a detector is connected to a mechanical system that allows it to move twice as much as the substrate (θ and 2θ), as shown in Fig. 4(a). Collecting the reflectance as a function of the angle, the refractive index of the substrate can be evaluated directly from Brewster's angle, which corresponds to the minimum value in reflectance.

Replacing the substrate with one with a thin homogenous Nafion film, a new reflectance signal is acquired, and, this time, the value to be analyzed is the angle where the intersection of both reflectance curves occurs, as depicted in Fig. 4(b). The tangent of this angle yields the refractive index of the film. To ensure the quality of the experiment, the refractive

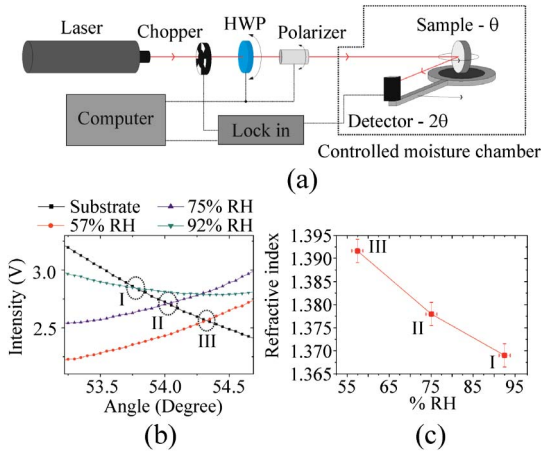

Fig. 4. (a) Experimental apparatus for refractive index determination by the Abelès method. The half-wave plate (HWP) as well as the polarizer were used to determine the right polarization state. (b) Reflectance curves for the bare substrate and substrate covered with Nafion thin film for three relative humidity values. (c) Moisture dependency of a 460 μm thick Nafion bulk refractive index.

index of a silica sample was measured 20 times with the setup just described and compared with the theoretical value from Sellmeier's equation, and it suggests that the accuracy of measurements is 5×10^{-4}, while the precision is 3×10^{-4}. After the calibration process, the system was ready to determine unknown refractive indices of thin films. After careful cleaning, microscope slides with back surface opaque, in order to avoid undesired reflection, were used as substrates for Nafion thin films. The films were prepared by spin coating with a typical spin rate of 600 rpm and average thickness of 460 μm. The entire setup was built inside a closed box, where the RH was varied. The procedure described above was repeated for three different values of RH: 57%, 75%, and 92%. For each of these values, different refractive indices were found: (1.392 ± 0.001), (1.378 ± 0.001), and (1.369 ± 0.001), respectively, at 633 nm, as shown in Figs. 4(b) and 4(c).

The analysis mentioned above concludes that Nafion can indeed be used as a transducer for a MKR-based humidity sensor. Considering that the device is completely surrounded by the polymer, the resonant wavelength displacement, $\Delta\lambda$, as a response of humidity step, $\Delta\gamma$, is given by the following expression:

$$\frac{\Delta\lambda}{\Delta\gamma} = \lambda_0 \left[\left(\frac{1}{n_{\text{eff0}}} \cdot \frac{\partial n_{\text{eff}}}{\partial n_{\text{out}}} \right) \frac{\Delta n_{\text{out}}}{\Delta\gamma} + \left(\frac{1}{L_{\text{cav0}}} \cdot \frac{\partial L_{\text{cav}}}{\partial\sigma} \right) \frac{\Delta\sigma}{\Delta\gamma} \right]. \tag{5}$$

The swelling and shrinkage tension moduli are represented by σ. The modal effective refractive index and the outer refractive index are represented, respectively, by n_{eff} and n_{out}. The first term on the right side represents the effect of the humidity over the effective mode index, and the second one describes the mechanical change of the knot, which results from the bulk swelling tension. Clearly, as discussed earlier, in the presence of humidity variation, $\Delta\sigma$ and Δn_{out} would change in opposition. In fact, the literature has reported, for a given sample, 17% of swelling, confronting less than 1% of refractive index change as a response to a step of 95% RH [36]. Hence, in Eq. (5), the variation from the stress term shall overcome the variation from the bulk refractive index change—as the coefficient B depends on the waveguide dispersion, and, in this case, it is weaker than the first term, which is purely morphological. Therefore, red shift ($\lambda > 0$) is expected for positive humidity steps.

B. MKR Humidity Sensor

So far, in the literature, among all fiber-based sensors, just a few optical humidity sensors have been demonstrated based on optical fiber resonators [19,20]. Wang *et al.* have assembled a polycrylamide microfiber loop humidity sensor with sensitivity as high as 490 pm/% RH [19].

The MKR sensor was assembled by casting a hydrophilic film on the knot with diameter of

250 μm. The film was prepared with a 5 wt. % Nafion solution (in low alcohols and 10% water), purchased from Aldrich and used as received. A drop of 3 μL was manually placed on the knot with the aid of a micropipette and left to dry for 24 h at room temperature. Figure 5(a) depicts the experimental setup for humidity measurements. The sensor was inserted into a glass chamber together with a hygrometer (Digisense humidity data logger model No. 37003-02), in order to provide the RH inside the chamber, allowing the calibration and characterization of the sensor (the calibration curve of the chamber is presented as an inset in Fig. 6). The chamber humidity was controlled by a gas blender, constituted by two mass flow controllers (Aalborg SDPROC TD 9704M) with flow rates ranging from 300 to 1000 mL · min^{-1}. Dry air was obtained by passing an air flow through desiccant columns of silica gel and molecular sieve 5 A (Sigma–Aldrich), while wet air was obtained by bubbling it into bubbling flasks containing distilled water. A proper mixture of these two air flows through a 1 m PTFE coil (0.4 mm internal diameter) was obtained before reaching the measuring chamber. A tunable laser source (from 1500 to 1600 nm) with a spectrometer with maximum resolution of 10 pm was used during the experiment to launch and collect the optical signal from the device.

The sensor indeed behaved in accordance with the predictions. When exposed to a humidity increase, its resonant wavelengths changed toward higher wavelengths, as shown in Fig. 5(c). This result suggests that the polymer expansion does not occur only on the normal substrate direction, as it occurs on SiO_2 Nafion thin film samples [36]. In such a situation

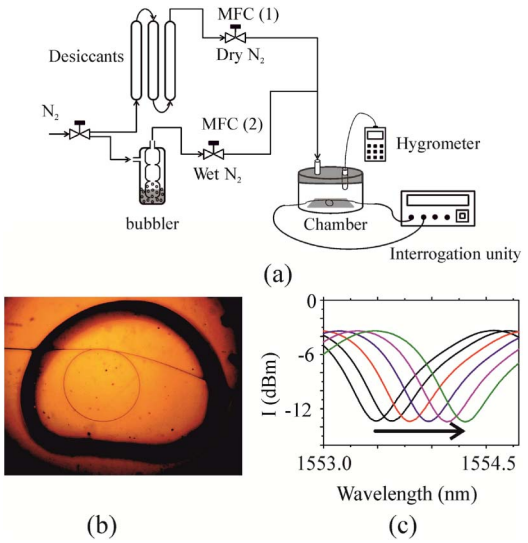

Fig. 5. (a) Experimental apparatus. N_2 was divided in humidified and dried flow streams electronically controlled by two mass flow controllers (MFCs). (b) Optical microscopy of a typical supported MKR embedded in Nafion. (c) Spectral response for humidity positivity change (experimental data). In response to an environmental humidity stimulus for greater values, the resonance peaks have displaced for greater wavelengths, as indicated by the arrow.

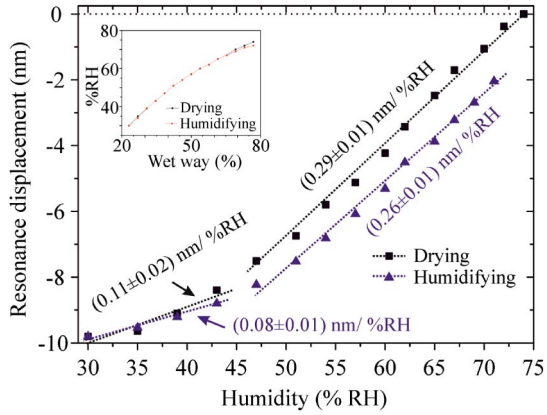

Fig. 6. Sensitivity curve of the MKR Nafion humidity sensor with the system humidity calibration curve as an inset.

(SiO_2), the plane swelling effect would be neglected, and, therefore, just the refractive index deviation would be taken into account—the second term of Eq. (5) would be ignored. This situation would result in a weakly sensitive sensor for humidity purposes. Hence, it suggests that the chosen substrate plays an important role in the sensor's response, since the structural parameter governs the physical effect over the refractive index change.

Table 2 shows the averaged spectral characteristics of the sensor in the presence of a RH level. The behavior of the FSR indicates that the effect of swelling governs the resonance dynamics when the RH is changed. Fluctuations in FWHM, Q-factor, finesse, and extinction ratio can be explained considering that the tensile forces change the coupler length and the local existence of water molecules induces scattering losses over the entire cavity region.

Sensitivity analysis, depicted in Fig. 6, has been performed and showed that there are two well-distinguished sensitive humidity regions. Initially, the humidity has been set to the maximum achievable value of the chamber, 75% RH. In the first part, the humidity was then gradually decreased to the minimum value and spectra were taken step by step. In the second part, the humidity was increased gradually to the maximum achievable value. At lower-mid humidity (30%–45% RH), two sensitivity values have been found, being (0.11 ± 0.02) nm/% RH when humidifying and (0.08 ± 0.01) nm/% RH when drying, while for higher-mid humidity (45% to 75% RH), (0.29 ± 0.01) nm/% RH for humidity increase and (0.26 ± 0.01) nm/% RH for humidity decrease. Device hysteresis of about 1.9 nm

Table 2. Averaged (over 1545–1555 nm) Spectral Characteristics as a Function of the Humidity Level

Humidity Level (% RH)	31	55	73
FSR (nm)	1.89	1.88	1.88
FWHM (nm)	0.95	0.99	0.95
$Q(\times 10^3)$	1.63	1.57	1.63
f	1.99	1.91	1.97
ε	5.84	6.36	5.30

has also been observed during the characterization, as shown in Fig. 6. Both results—hysteresis and two different sensitivity humidity ranges—are in accordance with the literature, of which, as reported, the Nafion has swelling hysteresis and anomalous water absorption in critical cases at highly dried and humidified cases [28].

In order to study the hysteresis, the sensor has been tested for two cycles, with three different humidity steps: 5%, 8%, and 11% RH. The results are depicted in Fig. 7(a), with the absolute hysteresis computed for each case [Fig. 7(b)]. For a step of 5% RH, after two complete cycles, an absolute hysteresis of 0.18 nm has been found, while, for 8% RH, 0.48 nm, and, for 11% RH, 1.6 nm. These results indicate, as expected, a dependency of the hysteresis over the applied humidity step.

Clearly, hysteresis, as discussed earlier, was expected in such a device as a consequence of the reported swelling hysteresis from bulk. Besides, as long as the water is absorbed from or released to the environment, the effective refractive index changes. The mechanism that could explain such behavior in the bulk Nafion is that this polymeric surrounding layer has both swelling and bulk refractive index as a function of the absorbed or released water. In that way, both stress and refractive index are local functions of these parameters, varying greatly over the layer's volume, which could produce a hysteresis factor as both water absorption and release are likely spatial stochastic processes.

Regarding its durability, the sensor lasted for more than 6 months, after several tryouts, without considerable optical loss and film degradation. The device, however, has shown poor resistance for time response testing. For several samples, the thin film has cracked during tests, whereas the RH was changed from the maximum achievable value to the minimum. Such a drawback is closely related to the interaction between the Nafion thin film and the substrate. Other sensors based on Nafion have performed such tests without any reported issues of this kind [17].

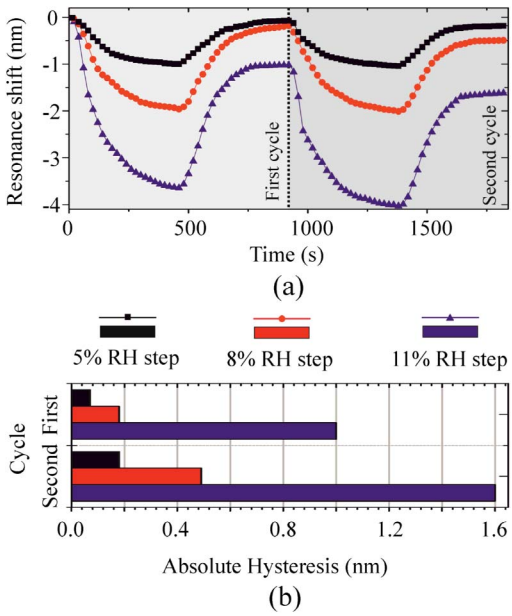

Fig. 7. (a) Analyzed hysteresis for a humidity cycle. (b) The absolute hysteresis rises with a larger humidity step, however, with apparent saturation.

4. Conclusion

A concept of an immersed MKR-based sensor has been presented. Fabrication methods as well as characterization of supported MKR have also been presented, including a procedure for determining unique coupling and total loss coefficients by comparing spectral responses in two well-known surrounding media. Particularly, the determination of those coefficients plays an important role in the development of resonant cavities for a wide range of applications, since the Q-factor could be tuned by varying the total losses. Such applications include laser cavities and high-Q sensors for precise measurements. For humidity sensing purposes, as silica MKR is insensitive to humidity change, a polymeric humidity responsive surrounding medium produced by Nafion has been used as a transducer.

Noticeable responses from the sensor regarded by the Nafion medium have been discussed, and later observed and measured, including spectral response and its main cause, expected hysteresis. It has been noticed that the spectrum displacement is directly connected to the tensile and compressive stress over the knot. As expected, two well-defined sensitive regions have been observed with sensitivity as high as (0.29 ± 0.01) nm/% RH for the high-mid humidity range and (0.11 ± 0.02) nm/% RH for the low-mid one. Moreover, time evolutional hysteresis has been studied and indicated strong relation with the applied humidity step value and possible saturation as well.

Future studies related to this device could be directed to better understanding the polymeric substrate and Nafion, since this interaction is a fundamental condition to achieve high sensitivity, as the material strain is far greater than that of the bulk refractive index change. Further studies can also be related to the development of methods to control the material hysteresis.

Marcelo Gouveia and Paloma Pellegrini gratefully acknowledge CNPq for their scholarships. Juliana Santos acknowledges a scholarship from FAPESP (grant 11/00322-2), and Ivo Raimundo acknowledges INCTAA (CNPq grant 573894/2008-6 and FAPESP grant 2008/57808-1) for financial support. The authors thank Dr. Felipe Beltran-Méjia for support during simulations, Claudecir Biazoli for thoughtful experimental discussions, and José Aparecido dos Santos for technical support.

References

1. A. N. Chryssis, S. M. Lee, S. B. Lee, S. S. Saini, and M. Dagenais, "High sensitivity evanescent field fiber Bragg

grating sensor," IEEE Photon. Technol. Lett. **17**, 1253–1255 (2005).
2. G. R. C. Possetti, L. C. Côcco, C. I. Yamamoto, L. V. R. De Arruda, R. Falate, M. Muller, and J. L. Fabris, "Application of a long-period fibre grating-based transducer in the fuel industry," Meas. Sci. Technol. **20**, 034012 (2009).
3. S. Silva, E. G. P. Pachon, M. A. R. Franco, J. G. Hayashi, F. X. Malcata, O. Frazão, P. Jorge, and C. M. B. Cordeiro, "Ultra-high-sensitivity temperature fiber sensor based on multimode interference," Appl. Opt. **51**, 3236–3242 (2012).
4. J. H. Osório, L. Mosquera, C. J. Gouveia, C. R. Biazoli, J. G. Hayashi, P. A. S. Jorge, and C. M. B. Cordeiro, "High sensitivity LPG Mach–Zehnder sensor for real-time fuel conformity analysis," Meas. Sci. Technol. **24**, 015102 (2013).
5. C. R. Biazoli, S. Silva, M. A. R. Franco, O. Frazão, and C. M. B. Cordeiro, "Multimode interference tapered fiber refractive index sensors," Appl. Opt. **51**, 5941–5945 (2012).
6. M. Sumetsky, Y. Dulashko, J. M. Fini, A. Hale, and D. J. DiGiovanni, "The microfiber loop resonator: theory, experiment, and application," J. Lightwave Technol. **24**, 242–250 (2006).
7. M. Sumetsky, "Optical fiber microcoil resonator," Opt. Express **12**, 2303–2316 (2004).
8. X. Jiang, L. Tong, G. Vienne, X. Guo, A. Tsao, Q. Yang, and D. Yang, "Demonstration of optical microfiber knot resonators," Appl. Phys. Lett. **88**, 223501 (2006).
9. M. A. Gouveia, T. Lee, R. Ismaeel, M. Ding, N. G. R. Broderick, C. M. B. Cordeiro, and G. Brambilla, "Second harmonic generation and enhancement in microfibers and loop resonators," Appl. Phys. Lett. **102**, 201120 (2013).
10. F. Xu, P. Horak, and G. Brambilla, "Optical microfiber coil resonator refractometric sensor," Opt. Express **15**, 7888–7893 (2007).
11. G. Y. Chen, T. Lee, R. Ismaeel, G. Brambilla, and T. P. Newson, "Resonantly enhanced Faraday rotation in an microcoil current sensor," IEEE Photon. Technol. Lett. **24**, 860–862 (2012).
12. W. Fan, Z. Zhang, J. Gan, X. Wei, H. Huang, S. Xu, and Z. Yang, "A wavelength tunable single frequency microfiber laser," Laser Phys. Lett. **11**, 015104 (2014).
13. L. H. Chen, C. C. Chan, T. Li, M. Shaillender, B. Neu, P. Balamurali, R. Menon, P. Zu, X. M. Ang, W. C. Wong, C. L. Poh, and K. C. Leong, "Chitosan-coated polarization maintaining fiber-based Sagnac interferometer for relative humidity measurement," IEEE J. Sel. Top. Quantum Electron. **18**, 1597–1604 (2012).
14. X. Yu, P. Childs, M. Zhang, Y. Liao, J. Ju, and W. Jin, "Relative humidity sensor based on cascaded long-period gratings with hydrogel coatings and Fourier demodulation," IEEE Photon. Technol. Lett. **21**, 1828–1830 (2009).
15. J. Yao, T. Zhu, D.-W. Duan, and M. Deng, "Nanocomposite polyacrylamide based open cavity fiber Fabry–Perot humidity sensor," Appl. Opt. **51**, 7643–7647 (2012).
16. I. M. Raimundo, Jr. and R. Narayanaswamy, "Evaluation of Nafion–Crystal Violet films for the construction of an optical relative humidity sensor," Analyst **124**, 1623–1627 (1999).
17. J. S. Santos, I. M. Raimundo, C. M. B. Cordeiro, C. R. Biazoli, C. A. J. Gouveia, and P. A. S. Jorge, "Characterisation of a Nafion film by optical fibre Fabry-Perot interferometry for humidity sensing," Sens. Actuators B **196**, 99–105 (2014).
18. I. M. Raimundo, Jr. and R. Narayanaswamy, "Simultaneous determination of relative humidity and ammonia in air employing an optical fibre sensor and artificial neural network," Sens. Actuators, B **74**, 60–68 (2001).
19. P. Wang, F. Gu, L. Zhang, and L. Tong, "Polymer microfiber rings for high-sensitivity optical humidity sensing," Appl. Opt. **50**, G7–G10 (2011).
20. Y. Wu, T. Zhang, Y. Rao, and Y. Gong, "Miniature interferometric humidity sensors based on silica/polymer microfiber knot resonators," Sens. Actuators B **155**, 258–263 (2011).
21. A. Omosebi and R. S. Besser, "Electron beam patterned Nafion membranes for DMFC applications," J. Power Sources **228**, 151–158 (2013).
22. F. Damay and L. C. Klein, "Transport properties of Nafion composite membranes for proton-exchange membranes fuel cells," Solid State Ionics **162–163**, 261–267 (2003).
23. H. Tang, S. Peikang, S. P. Jiang, F. Wang, and M. Pan, "A degradation study of Nafion proton exchange membrane of PEM fuel cells," J. Power Sources **170**, 85–92 (2007).
24. L. Xiao and T. A. Birks, "High finesse microfiber knot resonators made from double-ended tapered fibers," Opt. Lett. **36**, 1098–1100 (2011).
25. W. R. McKinnon, D. X. Xu, C. Storey, E. Post, A. Densmore, A. Delâge, P. Waldron, J. H. Schmid, and S. Janz, "Extracting coupling and loss coefficients from a ring resonator," Opt. Express **17**, 18971–18982 (2009).
26. F. Xu and G. Brambilla, "Embedding optical microfiber coil resonators in Teflon," Opt. Lett. **32**, 2164–2166 (2007).
27. G. Vienne, Y. Li, and L. Tong, "Effect of host polymer on microfiber resonator," IEEE Photon. Technol. Lett. **19**, 1386–1388 (2007).
28. K. S. Lim, A. A. Jasim, S. S. A. Damanhuri, S. W. Harun, B. M. A. Rahman, and H. Ahmad, "Resonance condition of a microfiber knot resonator immersed in liquids," Appl. Opt. **50**, 5912–5916 (2011).
29. F. Abelès, "La détermination de l'indice et de l'épaisseur des couches minces transparentes," J. Phys. Radium **11**, 310–314 (1950).
30. T. A. Birks and Y. W. Li, "The shape of fiber tapers," J. Lightwave Technol. **10**, 432–438 (1992).
31. M. Sumetsky, Y. Dulashko, J. M. Fini, and A. Hale, "Optical microfiber loop resonator," Appl. Phys. Lett. **86**, 161108 (2005).
32. S. Kedenburg, M. Vieweg, T. Gissibl, and H. Giessen, "Linear refractive index and absorption measurements of nonlinear optical liquids in the visible and near-infrared spectral region," Opt. Mater. Express **2**, 1588–1611 (2012).
33. G. Wang, P. P. Shum, L. Tong, C. M. Li, and C. Lin, "Polarization effects in microfiber loop and knot resonators," IEEE Photon. Technol. Lett. **22**, 586–588 (2010).
34. K. Morishita and T. Yamaguchi, "Wavelength tunability and polarization characteristics of twisted polarization beamsplitting single-mode fiber couplers," J. Lightwave Technol. **19**, 732–738 (2001).
35. K. A. Mauritz and R. B. Moore, "State of understanding of Nafion," Chem. Rev. **104**, 4535–4586 (2004).
36. S. Petrina, *Water Sorption, Viscoelastic, and Optical Properties of Thin Nafion Films* (Pennsylvania State University, 2013).